Photonic dual RF beam reception of an *X* band phased array antenna using a photonic crystal fiber-based true-time-delay beamformer

Harish Subbaraman,[1] Maggie Yihong Chen,[2] and Ray T. Chen[1,*]

[1]Microelectronics Research Center, Department of Electrical and Computer Engineering, University of Texas at Austin, Austin, Texas 78758, USA

[2]Omega Optics, Inc., 10435 Burnet Road, Suite 108, Austin, Texas 78758, USA

*Corresponding author: chen@ece.utexas.edu

Received 8 July 2008; revised 21 October 2008; accepted 29 October 2008; posted 30 October 2008 (Doc. ID 97957); published 27 November 2008

We report dual RF beam reception of an *X* band phased array antenna using a photonic crystal fiber (PCF)-based delay network. Each incoming RF signal can be independently received, and the angle of arrival can be determined based on the delay time-dependent wavelength. Two RF signals with frequencies 8.4 and 12 GHz impinge upon an *X*-band antenna array from −7.4° and −21.2°. These signals are detected, and the angle of arrival is determined with a very good degree of accuracy using PCF-based true-time delay. The total number of RF beams that can be simultaneously detected is limited by the hardware availability and the bandwidth of the wavelength differentiation capability of the system.

OCIS codes: 060.4005, 060.5295, 280.5110.

1. Introduction

Phased array antenna (PAA) is a key component in many of the modern military and commercial radar and communication systems. One of the advantages that this technology offers is a physical movement-free RF beam steering. However, electrical phase shifters are inherently narrowband. This calls for technologies that have a larger bandwidth and high immunity to electromagnetic interference. Optical true-time delay (TTD) techniques are capable of providing these features along with the ability to provide squint-free operation. Many optical schemes have been proposed to form a photonic feed for TTD. These include acousto-optic integrated circuit technique [1], Fourier optical technique [2], bulky optics techniques [3], dispersive fiber technique [4–8], fiber grating technique [9,10], and substrate-guided wave technique [11]. The dispersive fiber technique can provide a very compact and lightweight system. Conventional single-mode fiber (SMF) has a low value of dispersion, and so it is not a very good choice for this application, as long length of SMF is required to generate large delay values. However, highly dispersive fibers can reduce the overall length of the TTD lines as the required time delay can be generated in a very short length of such fibers.

Photonic crystal fibers (PCFs), with a periodic lattice of air holes running down the length of the fiber, can be designed to achieve very high dispersion values. A *W* index profile PCF, like the ones used in conventional dispersion compensation fibers [12], can be used to achieve high dispersion. PCFs with a dual-concentric core design have been designed to exhibit high dispersion coefficient values [13]. Our fabricated fiber design is also based on a dual-concentric core structure, and the dispersion value of the fiber is ~ -600 ps/nm/km, measured at a wavelength of 1550 nm, which is 33 times larger compared to that of a conventional SMF (~18 ps/nm/km at 1550 nm). Thus a shorter length of PCF compared

0003-6935/08/346448-05$15.00/0

to conventional SMF is required to generate the same amount of delay. This reduces the size and weight of the overall system.

In our previously reported research, PCF-based delay lines for a single RF beam steering was presented [14,15]. Recently we also demonstrated simultaneous multiple-beam transmission capability of our PAA system utilizing highly dispersive fibers [16]. In this paper we report with experimental confirmation the working principle of a photonic crystal-based TTD module with multiple-beam receiving capability for application in a PAA. Previous architectures used high-dispersion fibers with a dispersion coefficient of −88 ps/nm/km fibers [17,18]. Using our highly dispersive PCFs, the length of the TTD lines can be reduced by a factor of 7. In Section 2 we describe the setup and working principle of a general system for receiving multiple beams. In Section 3 we present our demonstration and experimental results for two beam operation at X band (8–12 GHz).

2. Optical Beam Former for Receiving Multiple Beams

Using the PCF-based TTD module, multiple-beam receiving can be realized by using the scheme as shown in Fig. 1. A general system is shown wherein a multiple number (M) of RF signals are received simultaneously using an antenna array with N elements through a single set of TTD lines.

A laser array is used to generate M different optical carrier waves with wavelengths λ_1 to λ_M. These optical carrier waves are combined together through a wavelength division multiplexer (WDM). The received RF signals from each antenna element modulate these optical carrier waves using electro-optic modulators (EOMs). The outputs of the N EOMs are connected to N TTD lines.

Each TTD line consists of different lengths of PCF (red section) and SMF (blue section), with the overall length of each TTD line being approximately equal and the lengths chosen in such a way that at a central wavelength of λ_0, the nominal delay through each TTD line is the same, and the outputs from the TTD lines for an RF signal incident normal on the antenna array are all in phase. At wavelengths greater than or less than λ_0, different time delays are induced in each TTD line, with a constant

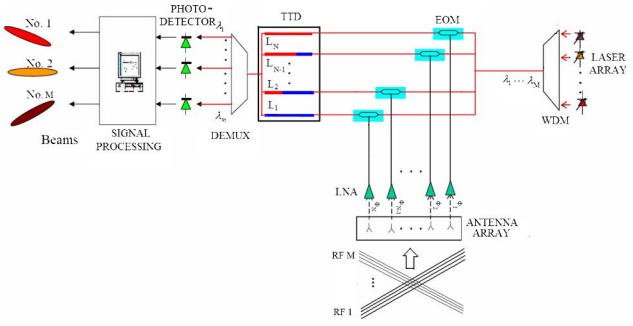

Fig. 1. (Color online) Structure of the receiving mode with multiple incoming beams. DEMUX, demultiplexer.

time-delay difference between adjacent channels at every wavelength. The time delay between adjacent lines induced by a beam received from an angle θ is given by [2]

$$\tau = \frac{d.\sin\theta}{c}, \tag{1}$$

where τ is the time-delay difference between adjacent lines, d is the antenna element spacing, and c is the speed of light in free space.

Suppose there are N TTD lines of length L having PCF segments of lengths $L_1, L_2, L_3 \ldots$ and L_N, respectively, as shown in Fig. 1. In practice, the first delay line consists of a SMF section of length L ($L_1 = 0$), and the Nth delay line consists of a PCF section of length L (no SMF section). The time delay generated in the ith delay line is given by

$$T_{\text{delay},i} = L_i \int_{\lambda_0}^{\lambda} D_{\text{PCF}}(\lambda)\mathrm{d}\lambda + (L - L_i)\int_{\lambda_0}^{\lambda} D_{\text{SMF}}(\lambda)\mathrm{d}\lambda,$$
$$i = 1, 2, 3, \ldots N. \tag{2}$$

The first term is contributed by the PCF section, and the second term is contributed by the conventional SMF. If we consider the difference of delay time, τ, between two adjacent fibers having PCF segments of lengths L_i and L_{i+1}, we have

$$\tau = (L_i - L_{i+1}).\int_{\lambda_0}^{\lambda}[D_{\text{PCF}}(\lambda) - D_{\text{SMF}}(\lambda)].\mathrm{d}\lambda,$$
$$i = 1, 2, 3 \ldots N - 1, \tag{3}$$

where τ is the time-delay difference between adjacent channels generated by λ with respect to λ_0.

Since the dispersion value of the PCF is much larger compared to that of the SMF for a fixed wavelength λ, the difference of time delays between different channels are only determined by the lengths of the PCFs. Therefore, by making the lengths of the PCF an arithmetic sequence, we can achieve equal time-delay differences between adjacent TTD lines at any given wavelength, thus forming a wavelength-tuned TTD line. Since multiple wavelengths are used for multiple incoming signals, the output signals from the TTD lines are fed to a wavelength division demultiplexer, where different optical wavelengths are separated. At any photodetector, say P_M, the signals corresponding to wavelength λ_M coming from all delay lines add up. In order for all the signals to add up constructively for the corresponding direction, the delay lines should alter the phase of signals in such a way that all signals arrive in phase at the photodetector. Since every wavelength generates one set of time delay values in the delay lines for a given angle of arrival, θ, only one wavelength would be able to compensate

phase differences between adjacent elements and deliver maximum power at the photodetector output.

The dispersion coefficient of the PCF at each wavelength is measured by measuring the time delay through the PCF at $\lambda \pm 0.1$ nm and dividing the time-delay difference by the length of PCF under test and wavelength span, $\Delta\lambda = 0.2$ nm. Figure 2 shows the measured second-order dispersion coefficient as a function of wavelength. The structural parameters of the PCF are chosen in order to have a phase-matched wavelength near 1550 nm. Around this wavelength, the PCF structure can achieve a peak dispersion coefficient of −600 ps/nm/km. By using a 3.5 m PCF length difference between adjacent TTD lines and selecting 1545 nm as the central wavelength, continuous time-delay values from −28.3 to +31.3 ps can be generated by tuning the wavelength continuously from 1530 to 1560 nm. Using the *X*-band array antenna with interelement spacing = 1.3 cm, also shown as an inset in Fig. 2, continuous beam steering from −41° to +46° can be achieved. Therefore, an incoming beam in the angular range of −41° to +46° can be detected, and the angle of arrival can be determined accurately. The relationship between the operating wavelength and calculated steering angle of the RF beam covering the *X* band (8–12 GHz) is also shown in the figure. This calculated result is later experimentally verified by detecting two beams impinging upon the *X*-band antenna array from two different angles. By having a lookup table in the signal processing unit showing the wavelength-angle relationship, the angle of arrival can be determined for any RF signal of interest due to the squint-free nature of the TTD lines [15]. Jiang *et al.* have shown the effects of thermal fluctuation on highly dispersive PCFs to be approximately 0.28% per °C from 21 °C to 80 °C [19]. The TTD network is placed in a temperature-controlled environment, and this leads to an insignificant shift in the beam steering angle. For a worst case temperature fluctuation of ±5 °C, the worst case error in the beam pointing direction is 1.5%.

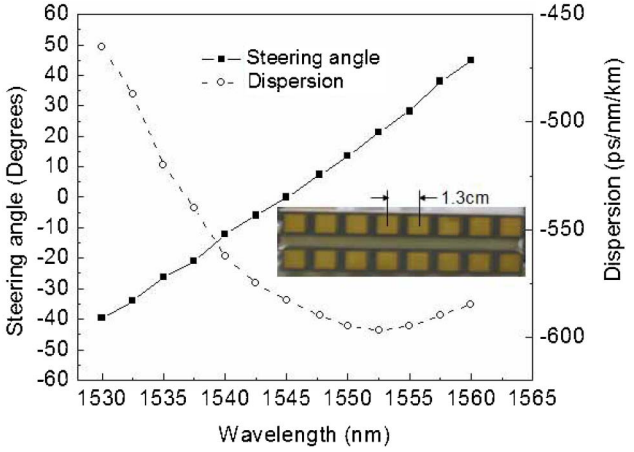

Fig. 2. (Color online) Solid curve shows the calculated steering angle of the beam as a function of wavelength. The dashed curve shows the measured dispersion coefficient of the PCF. The inset shows the *X*-band antenna array with an element spacing of 1.3 cm.

3. Demonstration of Two-Beam Receiving Operation

The schematic and actual experimental setup used for demonstrating two-beam receiving operation are shown in Fig. 3. We use two adjacent antenna elements, two modulators, and two adjacent delay lines in order to demonstrate dual-beam receiving capability.

We generated 8.4 and 12 GHz signals using an HP 8620C sweep oscillator and 8510C HP network analyzer, respectively. In order to show beam squint-free operation of the setup, the 8.4 and 12 GHz signals emitted by standard horn antennas were first placed at angles of −7.4° and −21.2°, respectively, with respect to the *X*-band antenna array normal and then at angles of −21.2° and −7.4°, respectively, with

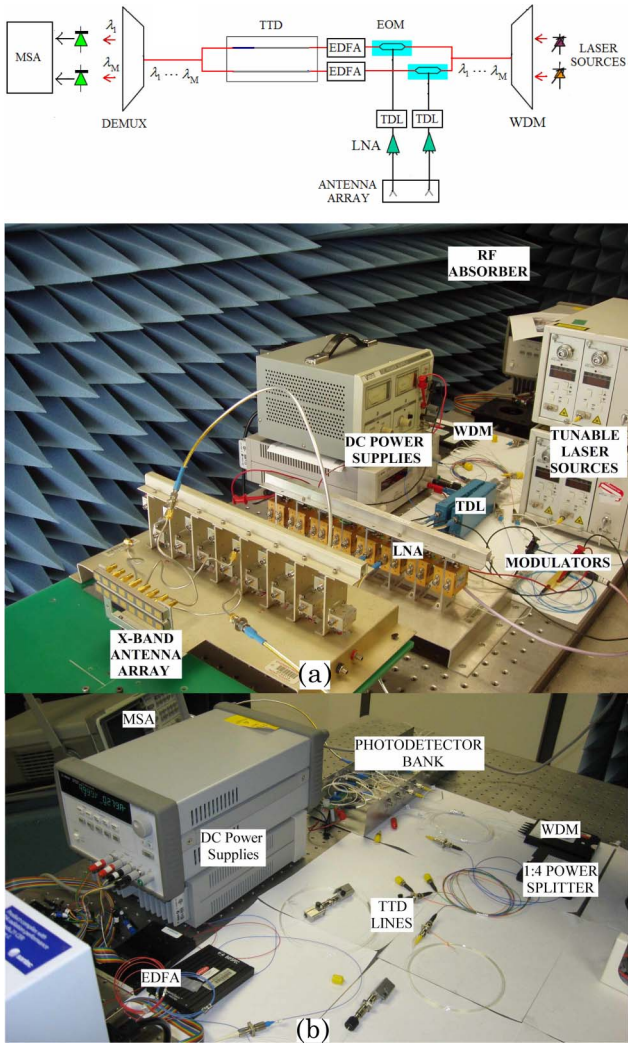

Fig. 3. (Color online) Schematic of the experimental setup. (a) Photograph showing the RF reception and electro-optical conversion section of the overall setup. (b) Photograph showing the TTD lines and signal processing section of the overall setup. The output from the modulators in (a) are connected to the inputs of EDFAs in (b). (The RF sources and the transmitting horn antennas of the setup are not shown.)

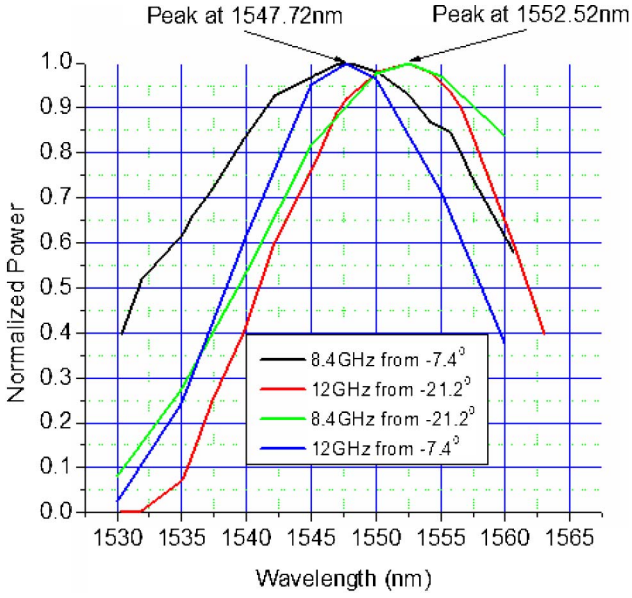

Fig. 4. (Color online) Signal power measured at the photodetector versus wavelength. The signal power peaks appear at 1547.72 nm for 8.4 and 12 GHz signals placed at −7.4° and at 1552.52 nm for 8.4 and 12 GHz signals placed at −21.2°.

respect to the X-band antenna array normal and at a distance of 2 m from the antenna array so that the emitting horn and the array antenna are in each other's far field. The antenna array consists of elements with a spacing of 1.3 cm. These external RF signals impinge on the antenna array, and the signals received are amplified using two low-noise amplifiers (LNAs) that have a gain of 35 dB. The tunable delay lines (TDLs) are used to fine-tune the delay through the lines for initial calibration of the setup. The amplified signals modulate the output signal of WDM, composed of combined optical wavelengths coming from two laser sources using two high-speed $LiNbO_3$ modulators. The tunable lasers have a maximum output power of 8 dBm. The optical signals are combined using a WDM. A maximum of 7 dB loss is encountered after passing through the modulator. The modulated optical signals are amplified using erbium-doped fiber amplifiers (EDFAs), which have a maximum output of 13 dBm and feed to two adjacent delay lines.

The two delay lines consist of 0 m of PCF with 10.5 m of SMF and 3.5 m of PCF with 7 m of SMF, respectively. The difference in the lengths of PCF sections between adjacent elements is 3.5 m. The overall length of each delay line is only 10.5 m. The maximum insertion loss due to the delay lines is 11 dB. The lengths of the SMF sections are trimmed such that at 1545 nm, the delays in each of the delay lines are equal. That is, for an RF signal incident normally on the antenna array, modulating a wavelength of 1545 nm, the signal detected at the photodetector will be a maximum. Therefore a different angle of arrival of RF signal will require a different wavelength to equalize the phase difference between adjacent elements in the TTD lines and generate a maximum at the photodetector output. In order to receive a beam from the positive θ direction, the experiment must be set up such that in the transmitting mode, the beam is steered in the negative θ direction.

The wavelengths are demultiplexed at the output of the delay lines and fed to a photodetector bank. A microwave spectrum analyzer (MSA) is used to monitor the detected RF output power from the photodetectors. Although one tunable laser source is sufficient to detect all of the impinging RF signals, one tunable laser source per RF signal will enable us to lock one signal with one tunable laser source while scanning for other signals using other laser sources. Therefore we use two tunable lasers for locking and detecting the 8.4 and 12 GHz signals independently. The wavelengths on the tunable lasers are tuned from 1530 to 1560 nm, and the outputs from the photodetectors are measured. The data are first measured for 8.4 and 12 GHz signal sources placed at −7.4° and −21.2°, respectively, and then measured for 8.4 and 12 GHz signal sources placed at −21.2° and −7.4°, respectively. The four measured data curves are shown in Fig. 4.

It can be clearly seen from the figure that at a wavelength of 1547.72 nm, there is a peak in the detected output power for 8.4 and 12 GHz signals arriving from −7.4°, and at a wavelength of 1552.52 nm, there is a peak in the detected power for 8.4 and 12 GHz signals arriving from −21.2°. These wavelengths correspond to complementary angles of 7.4° and 21.2°, respectively, in the transmission mode, which are also shown as two data points in Fig. 2, thus showing the multiple-beam receiving capability of our system. It can also be seen from Fig. 4 that there is no beam squint effect observed using the PCF-TTD technique. Since the wavelength on the tunable laser source can be tuned to within 0.01 nm accuracy, the error in determining the angle is very small. For example, for a change in 0.01 nm in the wavelength of the source at 1550 nm, the error in determining the angle is less than 0.027°, which corresponds to 0.2% error in determining the angle at 1550 nm. Although the peaks in Fig. 4 are distinguishable, by incorporating more numbers of adjacent elements to receive the impinging RF signals, we can achieve sharper peaks and distinguish very closely spaced signals.

This result is rather rudimentary with $N = 2$ elements due to hardware constraint in the laboratory. It is possible to scale the working principle to a larger array consisting of N antenna elements by using one modulator per antenna element and N TTD lines with the largest length of PCF equal to $(N-1) * 3.5$ m for PCF with dispersion coefficient of −600 ps/nm/km at 1550 nm. The easy scalability is due to the fact that a very long length of PCF can be fabricated in a single draw of the fiber, and the required lengths can be cut precisely from the spool. The cut lengths of PCF can then be spliced to SMFs in order to achieve the required TTD network consisting of N delay lines. The cost of the PCF-TTD

network is reduced as the number of delay lines is increased due to the shared cost of fiber fabrication. Such an "all-fiber" TTD system does not require intermediate electro-optic conversion and provides a very large bandwidth extending to several hundred gigahertz with beam squint-free operation. Apart from these advantages, the PCF-TTD network can also provide continuous beam-scanning capability.

Compared to other optical TTD techniques [1–10], this method provides a relatively compact and extremely low-weight feature with tremendous scope for scalability and extendability to two dimensions. Although conventional field-programmable gate array-based electronic counterparts are extremely dense, small in size, and cheaper with respect to the PCF approach, they suffer from beam-squint effect, and their operation is limited to several tens of gigahertz. By utilizing very highly dispersive PCFs, the length of PCF required, and hence the overall size and weight of the system, can be further reduced.

The operation can also be easily extended to two dimensions for (a) X–Y separable case by using two sets of PCF-TTD networks, one for each dimension as shown in [15] and (b) nonseparable X–Y case by making use of TTD networks in two dimensions and choosing the lengths of the PCF in the individual delay lines according to the location of the antenna element in the array. The received signal can then be processed by the signal processing unit to give the angle of arrival.

We are limited by the available hardware to conduct multiple-beam reception. In principle, the total number of RF beams that can be simultaneously detected is limited by the bandwidth ($\Delta\lambda$) of the WDM. As a result, hundreds of RF beams are detectable in the same time domain.

4. Conclusion

In conclusion, we present an optical beamformer based on highly dispersive fibers that can receive multiple beams simultaneously. Two-beam receiving operation is demonstrated using two optical carriers with different wavelengths, which generate two independent sets of time delays. Two incoming RF signals are simultaneously detected, and their angles of arrival are determined using the knowledge of the TTD lines. The TTD module is compact as the dispersion of the fabricated PCFs is as high as $-600\,\mathrm{ps/nm/km}$ at 1550 nm, and the system can be extended to receive many beams without increasing the overall complexity of the system.

This research is supported by the Defense Advanced Research Projects Agency (DARPA). We acknowledge helpful discussions with S. Pappert, R. Esman, and G. Brost. The assistance of P. Cao is also acknowledged. The antenna system used in the demonstrations is provided by the Air Force Research Laboratory, the Air Force Office of Scientific Research, and the Missile defense Agency.

References

1. L. H. Gesell, R. E. Feinleib, J. L. Lafuse, and T. M. Turpin, "Acousto-optic control of time delays for array beam steering," Proc. SPIE **2155**, 194–204 (1994).
2. G. A. Koepf, "Optical processor for phased-array antenna beam formation," Proc. SPIE **477**, 75–81 (1984).
3. N. A. Riza, "Liquid crystal-based optical time delay units for phased array antennas," J. Lightwave Technol. **12**, 1440–1447 (1994).
4. R. Soref, "Optical dispersion technique for time-delay beam steering," Appl. Opt. **31**, 7395–7397 (1992).
5. R. D. Esman, M. J. Monsma, J. L. Dexter, and D. G. Cooper, "Microwave true time-delay modulator using fibre-optic dispersion," Electron. Lett. **28**, 1905–1907 (1992).
6. R. D. Esman and L. Goldberg, "Fiber optic true time delay array antenna feed system," U.S. patent 6,337,660 (January 8, 2002).
7. M. Y. Frankel, P. J. Matthews, and R. D. Esman, "Fiber optic true time steering of an ultrawideband receive array," IEEE Trans. Microwave Theory Tech. **45**, 1522–1526 (1997).
8. M. Y. Frankel, R. D. Esman, and M. G. Parent, "Phased-array transmitter/receiver controlled by a true time-delay fiber-optic beamformer," IEEE Photonics Technol. Lett. **7**, 1216–1218 (1995).
9. A. Moloney, C. Edge, and I. Bennion, "Fiber grating time delay elements for phased array antennas," Electron. Lett. **31**, 1485–1486 (1995).
10. J. E. Roman, M. Y. Frankel, P. J. Matthews, and R. D. Esman, "Time-steered array with a chirped grating beamformer," Electron. Lett. **33**, 652–653 (1997).
11. Y. Chen and R. T. Chen, "A fully packaged true time delay module for a K-band phased array antenna system demonstration," IEEE Photonics Technol. Lett. **14**, 1175–1177 (2002).
12. U. Peschel, T. Peschel, and F. Lederer, "A compact device for highly efficient dispersion compensation in fiber transmission," Appl. Phys. Lett. **67**, 2111–2113 (1995).
13. F. Gerome, J. L. Auguste, and J. M. Blondy, "Design of dispersion-compensating fibers based on a dual-concentric-core photonic crystal fiber," Opt. Lett. **29**, 2725–2727 (2004).
14. Y. Jiang, B. Howley, Z. Shi, Q. Zhou, R. T. Chen, M. Y. Chen, G. Brost, and C. Lee, "Dispersion-enhanced photonic crystal fiber array for a true time-delay structure X-band phased array antenna," IEEE Photonics Technol. Lett. **17**, 187–189 (2005).
15. Y. Jiang, Z. Shi, B. Howley, X. Chen, M. Y. Chen, and R. T. Chen, "Delay time enhanced photonic crystal fiber array for wireless communications using 2-D X-band phased-array antennas," Opt. Eng. **44**, 125001 (2005).
16. M. Y. Chen, H. Subbaraman, and R. T. Chen, "Photonic crystal fiber beamformer for multiple X-band phased-array antenna transmissions," IEEE Photon. Technol. Lett. **20**, 375–377 (2008).
17. P. J. Matthews, M. Y. Frankel, and R. D. Esman, "A wideband fiber optic true time steered array receiver capable of multiple independent simultaneous beams," IEEE Photonics Technol. Lett. **10**, 722–724 (1998).
18. P. J. Matthews, M. Y. Frankel, and R. D. Esman, "A wideband fiber optic true time steered array receiver capable of multiple independent simultaneous beams," IEEE Photonics Technol. Lett. **10**, 722–724 (1998).
19. Y. Jiang, X. Chen, B. Howley, M. Y. Chen, and R. T. Chen, "Effects of thermal fluctuation on highly dispersive photonic crystal fibers," Appl. Phys. Lett. **88**, 011108 (2006).